CIP2A promotes bronchiolitis obliterans by activating the NF-κB pathway

XU ZHOU[1], XINGYOU ZHAO[2], YANNING LI[1] and BAOQING ZHANG[1]

[1]Department of Pediatrics, Affiliated Hospital of Shandong University of Traditional Chinese Medicine, Jinan, Shandong 250011, P.R. China; [2]The First College of Clinical Medicine, Shandong University of Traditional Chinese Medicine, Jinan, Shandong 250355, P.R. China

Received July 29, 2024; Accepted January 20, 2025

DOI: 10.3892/mmr.2025.13473

Abstract. Bronchiolitis obliterans (BO) is a destructive fibrotic lung disease, which can be partly induced by 2,3-butanedione [also known as diacetyl (DA)]; however, the mechanism underlying the effects of DA on BO is not clear. In the present study, a bioinformatics analysis was performed using DA-treated or untreated lung tissues of rats, and it was observed that cell proliferation regulating inhibitor of protein phosphatase 2A (CIP2A) was significantly increased in samples from the DA group. CIP2A is associated with inflammation and epithelial-mesenchymal transition (EMT), and facilitates lung injury; however, its effect on DA-induced BO and the underlying mechanism remain unknown. To solve these issues, DA-treated models of BO were established in rats and cells, and ethoxysanguinarine (a CIP2A inhibitor) was administered to induce a decrease in CIP2A. The pathological changes were detected by hematoxylin and eosin, Masson and Giemsa staining. Reverse transcription-quantitative PCR, western blotting, immunohistochemistry, immunofluorescence and enzyme-linked immunosorbent assay were used to measure CIP2A expression and levels of pathology-related markers. Notably, inhibition of CIP2A ameliorated the pathological features of BO, including reduced intraluminal occlusion, inflammatory infiltration and fibrosis. The expression of inflammation, fibrosis and EMT markers was also decreased in samples with CIP2A inhibition. Furthermore, CIP2A inhibition was revealed to work through the nuclear factor-κB (NF-κB) pathway; phosphorylation of NF-κB inhibitor α and nuclear translocation of p65 were reduced. In summary, these results demonstrated that CIP2A may promote BO development by increasing inflammation, fibrosis and EMT through activating the NF-κB signaling pathway. Therefore, inhibition of CIP2A may be considered a potential strategy for BO treatment.

Correspondence to: Dr Xu Zhou, Department of Pediatrics, Affiliated Hospital of Shandong University of Traditional Chinese Medicine, 42 Wenhua West Road, Jinan, Shandong 250011, P.R. China
E-mail: 71001885@sdutcm.edu.cn

Key words: cell proliferation regulating inhibitor of protein phosphatase 2A, bronchiolitis obliterans, fibrosis, inflammation, epithelial-mesenchymal transition, nuclear factor-κB

Introduction

Bronchiolitis obliterans (BO) is a destructive fibrotic lung disease induced by lower respiratory lesions (1,2). The pathological features of BO include intraluminal granulation accumulation, progressive airflow obstruction, inflammation and fibrosis of airway epithelial cells, collagen and matrix deposition, and epithelial-mesenchymal transition (EMT) exacerbation (3-7). Although various modalities have been applied in stopping or slowing down the progression of BO, no method has yet been proven to reverse established BO (4,8). The survival rate of patients with BO is poor; the 5-year survival rate is ~40% (4,8); therefore, it is of great significance to identify potential therapeutic targets of BO.

Even though the exact pathogenesis of BO is unclear, lung transplantation, severe respiratory tract infections and inhalation exposures to certain chemicals are considered to be potential causes (9,10). Notably, 2,3-butanedione [also known as diacetyl (DA)] is a volatile α-diketone, which is added to popcorn, flavoring and e-cigarettes due to its buttery aroma (10-12). In 2002, Kreiss *et al* (13) reported that inhaling the volatile butter-flavored ingredient DA was the main cause of BO occurring in popcorn factory workers. Over the past few decades, numerous studies have certified that DA is strongly associated with the development of BO (10-12,14). Notably, DA is used as a chemical flavoring in a number of fields and knowledge on how it results in BO remains in its infancy.

Cell proliferation regulating inhibitor of protein phosphatase 2A (CIP2A) is a dysregulated protein in several types of cancer, including breast cancer, colorectal cancer, bladder cancer and hepatocellular carcinoma, which can affect cell proliferation, cell cycle progression, apoptosis and tumor formation (15-17). In addition, CIP2A serves a critical role in nerve diseases, such as inhibiting depression-like behaviors and promoting the development of Alzheimer's disease (18-20). The expression of EMT markers, including Snail, Vimentin and E-cadherin, has been shown to be regulated by CIP2A (21,22). Furthermore, in a previous study, the stronger the local inflammation in cancer, the more CIP2A was detected (23). These findings indicated that CIP2A may

mediate EMT and inflammation. Moreover, in human primary bronchial epithelial cells (HPBECs) isolated from patients with chronic obstructive pulmonary disease, CIP2A was shown to be highly expressed and this enhancement contributed to a loss of lung function (24). However, the effect of CIP2A on BO is currently unclear.

The present study aimed to assess the effects of CIP2A on BO and its underlying mechanism. The findings suggested the potential of CIPA2 as a new target for BO treatment.

Materials and methods

Animals and groups. Male Sprague Dawley rats (age, 8 weeks; weight, 300 g) were purchased from Changsheng Bio-Technology Co., Ltd. Rats received 1 week of environmental adaptation (22±1˚C; 45-55% humidity; 12-h light/dark cycle), and had *ad libitum* access to water and food. A total of 79 rats were used in the present study. For experiment 1, 12 rats were included in the control group and 13 rats in the DA group (one of the 13 rats died naturally during the modeling process); in experiment 2 ,12 rats were included in the control group, 14 rats in the DA group (two of the 14 rats died naturally during the modeling process), 14 rats in the DA + vehicle group (one of the 14 rats died naturally during the modeling process and one rat was used in a preliminary experiment to determine the antibody concentration required and the detection conditions of the kit), and 14 rats in the DA + Eth group (one of the 14 rats died naturally during the modeling process and one rat was used in a preliminary experiment to determine the antibody concentration required and the detection conditions of the kit). Six rats were used to collect bronchoalveolar lavage fluid (BALF) in each group and another six rats were used for other experiments. The groups were treated as follows: i) Control group, intratracheal instillation of aseptic distilled water; ii) DA group, intratracheal instillation of 125 mg/kg DA (Shanghai Macklin Biochemical Co., Ltd.); iii) DA + vehicle group, subcutaneous injection with solvent (10% DMSO + 90% corn oil); iv) DA + ethoxysanguinarine (Eth; inhibitor of CIP2A) group, subcutaneous injection with 0.35 mg/kg Eth (Shanghai Macklin Biochemical Co., Ltd.) (25). For BO modeling *in vivo*, the protocols described in Palmer *et al* (11) and House *et al* (26) were performed with minor modifications; the rats in the last three groups accepted DA intratracheal instillation once a day for 7 days. Firstly, the rats were anesthetized using isoflurane (3% to induce anesthesia and 2% to maintain anesthesia). For intratracheal instillation, the rat was placed supine on a flat plate at an angle of 30-40˚ and the tongue was pulled out. A cannula was inserted into the trachea and DA from the injector was injected slowly into the trachea via cannula; the instillation lasted ~5 min. The control rats received aseptic distilled water. On day 8, rats in the DA + vehicle and DA + Eth groups were treated with solvent or Eth once a day for 4 weeks. The rats in the control and DA groups received normal saline. After 4 weeks, the rats were sacrificed with CO_2 (60% replacement rate), and BALF, and left and right lung tissues with bronchi were collected. Animal death was confirmed by the absence of toe pinching reflex, breathing and heartbeat. A humane endpoint was reached when rats lost weight quickly, or experienced a decline in their physical health, such as a lack or loss of appetite, lethargy or persistent recumbency. No animal reached these humane endpoints before the end of the experiment. The present animal experiments were performed following the Guideline for the Care and Use of Laboratory Animals (27) and were approved by the Experimental Animal Ethics Committee of Affiliated Hospital of Shandong University of Traditional Chinese Medicine [approval number: (2023) No. 163 application for provincial natural basic experiment; Jinan, China].

mRNA-sequencing (mRNA-seq). After isolating mRNA from rat lung tissues with bronchi using TRIzol® (cat. no. 15596018CN; Invitrogen; Thermo Fisher Scientific, Inc.), and passing integrity and total quantity testing, mRNA was used to synthesize cDNA. Amplification was carried out via PCR, followed by purification using AMPure XP Beads (Beckman Coulter, Inc.). The type of sequencing, including nucleotide length and the direction of sequencing, were as follows: Nucleotide length, 150 bp; direction of sequencing, paired end. Library quality was detected using an Agilent 2100 system (Agilent Technologies, Inc.). The loading concentration of the final library was >2 nM, which was measured by quantitative PCR (qPCR). The NovaSeq 6000 Illumina high-throughput sequencing platform (Illumina, Inc.) was used to sequence the library. with the sequencing kit NovaSeq 6000 S4 Reagent Kit (cat. no. 20028312; Illumina, Inc.). Differentially expressed genes (DEGs) were defined as absolute value of log2 fold change (FC) >1.5 and adjusted-P<0.001. The P-value was adjusted through the Benjamini-Hochberg method using DESeq2 software. DESeq2 (1.24.0) (28) was used to analyze the data. Gene Ontology (GO) analysis was performed using org.Rn.eg.db Version 3.19.1 (https://bioconductor.org/packages/release/data/annotation/html/org.Rn.eg.db.html) and clusterProfiler Version 4.12.0 (https://bioconductor.org/packages/release/bioc/html/clusterProfiler.html). Five gene name lists were downloaded, which were associated with apoptosis, inflammation, fibrosis, EMT and the epithelium, from GeneCards (https://www.genecards.org/). According to the description of the protein on GeneCards, they were divided into 12 types.

Reverse transcription-qPCR. Total RNA was isolated from tissues using TRIpure (BioTeke Corporation). RNA then was converted to cDNA using the All-in-One First-Strand SuperMix (Magen Biotechnology Co., Ltd.) according to the manufacturer's instructions. qPCR was performed with 2X Taq PCR MasterMix (Beijing Solarbio Science & Technology Co., Ltd.) and SYBR Green (Beijing Solarbio Science & Technology Co., Ltd.). The thermocycling conditions were as follows: The sample was first incubated at 95˚C for 5 min; followed by 40 cycles at 95˚C for 10 sec at 60˚C for 10 sec and 72˚C for 15 sec. The sample was then incubated at 72˚C for 1 min 30 sec, at 40˚C for 1 min, and then the melting process was carried out, gradually increasing the temperature from 60˚C to 94˚C, with a rate of 1˚C increase every second. Finally, the sample was incubated at 25˚C for 1-2 min. β-actin was used as an endogenous control and data were calculated using the $2^{-\Delta\Delta Cq}$ method (29). The following primers were used for amplification: CIP2A forward, 5'-TTGTCGGGAGTGGTTTG-3', reverse, 5'-AGGGCATAGTTAGCTCATCTT-3'; solute carrier family 1 member 6 (SLC1A6) forward, 5'-TCCTGA

TTGCTGGAAAGA-3', reverse, 5'-CGGAAAGTGATAGGC AGA-3'; endoplasmic reticulum to nucleus signaling 2 (ERN2) forward, 5'-TACACCGTGACCTCAAGCC-3', reverse, 5'-TGC CGGGAATACCAGAAT-3'; ribonuclease A family member 2 (RNASE2) forward, 5'-GCCATCCAGCACATCTA-3', reverse, 5'-TGTACTTCTCCCGTCTTTA-3'; tryptase β2 (TPSB2) forward, 5'-ATTGTGGGAGGACGAGA-3', reverse, 5'-CTG TGGGTGAATGAGGG-3'; and β-actin forward, 5'-GGAGAT TACTGCCCTGGCTCCTAGC-3' and reverse, 5'-GGCCGG ACTCATCGTACTCCTGCTT-3'.

Hematoxylin and eosin (H&E) staining. Tissues were obtained from the rats after euthanasia, and were fixed with 4% paraformaldehyde at room temperature for >24 h, dehydrated with different concentrations of ethanol, permeabilized with xylene for 30 min at room temperature, embedded in paraffin and cut into slices (5 μm). The slices were then stained with H&E and their images were captured using a BX53 fluorescence microscope (Olympus Corporation). Briefly, slices were incubated with hematoxylin solution for 5 min and were then differentiated with 1% hydrochloric acid alcohol, before being soaked in eosin for 3 min at room temperature. The measurement of severity score was performed as previously described (30). Briefly, severity was scored as follows: Normal lung, 0 points; slight fibrous thickening of the alveolar or bronchial wall, 1 point; moderate thickening of lung wall without marked damage to lung structure, 2-3 points; worsening fibrosis with obvious damage to lung architecture and the formation of fiber bands or small fiber clumps, 4-5 points; serious structural deformation, a large fiber area including honeycombing, 6-7 points; complete fiber occlusion of the field, 8 points.

Masson's trichrome staining. Masson staining was used to measure fibrosis with the Masson kit (Leagene; Beijing Regen Biotechnology Co., Ltd.). Briefly, the aforementioned paraffin-embedded tissue slices were incubated with Ponceau-Magenta for 10 min. After treating with phosphomolybdic acid for 2 min, the slices were stained with aniline blue for 1 min. All steps were carried out at room temperature. The images were obtained using a BX53 microscope. The collagenization area was measured based on a previous study (31).

Giemsa staining. The BALF was collected and part of it was used for detecting total cell count using a hemocytometer. The remaining BALF was used for differential counting of inflammatory cells. Giemsa staining at room temperature for 1 min with Giemsa A and for 7 min with Giemsa B (Giemsa Staining Kit; Nanjing Jiancheng Bioengineering Institute) was carried out to manually measure the number of different types of cells under a DP73 fluorescence microscope (Olympus Corporation), including macrophages, lymphocytes, neutrophils and eosinophils.

Immunohistochemistry. The aforementioned paraffin-embedded tissue slices were dewaxed with xylene, rehydrated in a descending alcohol series and underwent antigen retrieval at 100˚C in antigen repair solution (9 ml citric acid buffer, 41 ml sodium citrate buffer mixed with 450 ml distilled water) for 10 min and were then cooled before being incubated with 3% H_2O_2 for 15 min to eliminate endogenous peroxidase activity at room temperature. After blocking with 1% BSA (Sangon Biotech Co., Ltd.) for 15 min at 4˚C, the slices were incubated with CIP2A antibody (1:100; cat. no. bs-5948R; BIOSS) overnight at 4˚C and with Goat Anti-Rabbit IgG/HRP (1:100; cat. no. SE134; Beijing Solarbio Science & Technology Co., Ltd.) for 45 min. Diaminobenzidine was used as a chromogenic substrate and the nuclei were counterstained using hematoxylin at room temperature for 3 min. The images were captured under a BX53 microscope. Relative protein levels were determined as follows: Relative level=integrated optical density/area. The CIP2A immunohistochemistry staining was validated using an isotype control (data not shown).

In vitro model. HPBECs were purchased from iCell Bioscience Inc. and were cultured in the HPBECs cultivation system (iCell Bioscience Inc.). The *in vitro* model of BO was established as previously described (32). Cells were exposed to DA (25 mM) for 1 h on days 0, 2 and 4, and were treated with Eth (GLPBIO Technology LLC) for 24 h on day 6 at 37˚C. For Eth intervention dose *in vitro,* Jin *et al* (25) and Liu *et al* (33) were referred to, and the concentrations of Eth were set to 2, 4 and 6 μM.

Western blotting. Proteins were harvested from tissues and cells using radio immunoprecipitation assay lysis buffer (Proteintech Group, Inc.), or the nuclear protein and cytoplasmic protein extraction kit (Proteintech Group, Inc.). Protein concentrations were measured using the Bicinchoninic Acid Protein Assay Kit (Proteintech Group, Inc.). Proteins (15-30 μg/15 μl/lane) were separated by sodium dodecyl sulfate polyacrylamide gel electrophoresis (5% stacking gel; 8, 10 or 12% separation gel) and were then transferred to polyvinylidene fluoride membranes, following by blocking using Western Blocking Buffer (Proteintech Group, Inc.). The membranes were then incubated with primary antibodies overnight at 4˚C and with secondary antibodies for 40 min at 37˚C. Visualization was conducted with ECL Western Blotting Substrate (Proteintech Group, Inc.). The following antibodies (Proteintech Group, Inc.) were used in the present study: CIP2A monoclonal antibody (cat. no. 67843-1-Ig; 1:10,000), α-smooth muscle actin (α-SMA) polyclonal antibody (cat. no. 14395-1-AP; 1:1,000), fibronectin polyclonal antibody (cat. no. 15613-1-AP; 1:10,000), Snail polyclonal antibody (cat. no. 13099-1-AP; 1:10,000), inducible NO synthase (iNOS) polyclonal antibody (cat. no. 22226-1-AP; 1:500), NF-κB inhibitor α (IκBα) polyclonal antibody (cat. no. 10268-1-AP; 1:20,000), phosphorylated-IκBα (p-IκBα; Ser32/36) recombinant antibody (cat. no. 82349-1-RR; 1:20,000), p65 polyclonal antibody (cat. no. 10745-1-AP; 1:3,000), HRP-conjugated Affinipure goat anti-rabbit IgG(H+L) (cat. no. SA00001-2; 1:10,000), HRP-conjugated Affinipure rabbit anti-goat IgG(H+L) (cat. no. SA00001-4; 1:10,000), HRP-conjugated Affinipure goat anti-mouse IgG(H+L) (1:10,000), Histone-H3 polyclonal antibody (cat. no. 17168-1-AP; 1:2,000) and β-actin monoclonal antibody (cat. no. 66009-1-Ig; 1:20,000). β-actin was used as an internal control and Histone-H3 was used as a nuclear loading control.

Immunofluorescence. The aforementioned paraffin-embedded tissue slices and cell sections were used for immunofluorescence

analysis. Antigen retrieval was performed for 10 min on tissue slices with antigen repair solution (9 ml citric acid buffer, 41 ml sodium citrate buffer mixed with 450 ml distilled water) at 100˚C and permeabilization was carried out on cell sections with 0.1% Triton X-100 for 30 min at room temperature. After blocking with BSA for 15 min at room temperature, the slices and sections were incubated with primary antibodies and a secondary antibody. The antibodies used in this analysis included Vimentin (cat. no. AF7013; 1:200) and E-cadherin (cat. no. AF0131; 1:200) primary antibodies (Affinity Biosciences), and Cy3-conjugated Goat Anti-Rabbit IgG (H+L) (1:200; cat. no. SA00009-2; Proteintech Group, Inc.). The PBS was used as dilution. Subsequently, the nuclei were stained with DAPI and the images were obtained using a BX53 fluorescence microscope.

Enzyme-linked immunosorbent assay (ELISA) kit. The levels of interleukin (IL)-1β, IL-6 and tumor necrosis factor (TNF)-α were detected using ELISA kits according to the manufacturer's instructions. All ELISA kits (cat. nos. EK301B, EK101B, EK306, EK106, EK382 and EK182) were provided by Multi Sciences (Lianke) Biotech Co., Ltd. The ELX-800 microplate reader (Bio-Tek Instruments, Inc.) was used to measure absorbance.

Statistical analysis. GraphPad (version 9.5.0; Dotmatics) was used for data analysis. Comparisons among groups were statistically analyzed using unpaired Student's t-test (two groups) or one-way ANOVA (four groups) with Tukey's multiple comparison test. The severity score was analyzed with nonparametric tests, either Mann-Whitney test or Kruskal-Wallis test with Dunn's multiple comparisons test. $P<0.05$ was considered to indicate a statistically significant difference.

Results

DA induces symptoms of BO in Sprague Dawley rats. A DA-induced rat model of BO was established to carry out the following experiments (Fig. 1A). As shown in Fig. 1B, more evident fibrosis accompanied by more extensive inflammatory infiltration was observed in the airway of rats that underwent endotracheal instillation with DA compared with in the control rats. DA also caused partial blockages in the airways compared with distilled water, and higher severity scores were observed in the DA group. The Masson's trichrome staining results of healthy and DA-treated tissues demonstrated that larger levels of collagenous fiber were present in model tissues compared with those in healthy tissues (Fig. 1C). Occlusion was also found in the DA group according to Masson staining, which was in line with the results of H&E staining. To quantify the effects of DA on inflammatory infiltration, inflammatory cells were counted in the BALF (Figs. 1D and S1A). The numbers of macrophages, neutrophils, lymphocytes, eosinophils and total cells in the BALF were significantly increased in the BO model rats compared with those in the control rats. These results indicated that the *in vivo* BO model was successfully established.

CIP2A expression is increased in DA-treated rats. In order to explore the related molecular mechanism of BO, high-throughput analysis was conducted using the lung tissues of rats. There were 150 upregulated DEGs and 55 downregulated DEGs in tissues from the DA group compared with in normal tissues (Fig. 2A). RT-qPCR was carried out to verify the results of mRNA-seq that SLC1A6 and ERN2 were increased, and RNASE2 and TPSB2 were reduced in samples from the DA group (Fig. 2B). GO outcomes revealed that DEGs were enriched in apoptosis, inflammation, fibrosis, EMT and epithelium-associated items, including 'negative regulation of neutrophil apoptotic process', 'endothelial cell apoptotic process', 'cyclin A2-CDK2 complex', 'cyclin B1-CDK1 complex', 'cyclin-dependent protein kinase holoenzyme complex', 'DNA replication origin binding', 'cyclin-dependent protein serine/threonine kinase regulator activity', 'DNA helicase activity', 'regulation of leukotriene production involved in inflammatory response', 'regulation of inflammatory response', 'interleukin-8 receptor activity', 'immune receptor activity', 'fibroblast proliferation', 'response to fibroblast growth factor', 'elastic fiber', 'banded collagen fibril', 'contractile fiber', 'regulation of epithelial to mesenchymal transition', 'collagen metabolic process', 'collagen-containing extracellular matrix', 'fibronectin binding', 'epithelium regeneration' and 'epithelium migration' (Fig. 2C), indicating that BO may be related to them. Therefore, five datasets were downloaded, which were associated with apoptosis, inflammation, fibrosis, EMT and the epithelium, from GeneCards, and a Venn analysis was conducted using these datasets and the identified DEGs. As shown in Fig. 2D, only 47 DEGs simultaneously existed in the six datasets (the five datasets provided by GeneCards and the present mRNA-seq results). Proteins encoded by the 47 DEGs were divided into 12 categories, including functional protein, constitutive protein, receptor, binding protein, enzyme, cyclin, glycoprotein, growth factor, proteoglycan, transcription factor, cytokines and chemokines (Fig. 2E). The present study subsequently focused attention on functional proteins. Among these functional proteins, CIP2A, located on chromosome 11, was increased in DA-treated lung tissues (Fig. 2F). The results of RT-qPCR, western blotting and immunohistochemistry verified the mRNA-seq results that CIP2A was higher in DA-treated rats than that in control rats (Fig. 3A-C). Based on these findings, it may be hypothesized that the development of BO is related to several factors and CIP2A may serve an important role during this process.

Inhibiting CIP2A attenuates the injuries induced by DA in the bronchus and lung of rats. To evaluate the effect of CIP2A inhibition on BO, Eth, a CIP2A inhibitor, was injected subcutaneously into DA-treated rats (Fig. 4A). DA induced airway and alveolar injury compared with that in control rats; however, the fibrosis, inflammatory infiltration and blocking that were induced by DA were reversed after suppressing CIP2A (Fig. 4B). As shown in Fig. 4C, more collagen deposition was detected in the BO group than that in the control mice, whereas collagen deposition was reduced when CIP2A was inhibited. The number of macrophages, lymphocytes, neutrophils and total cells in animals with CIP2A reduction was decreased compared with that in the DA group (Figs. 4D and S1B), suggesting that CIP2A may serve a role by recruiting inflammatory cells, especially lymphocytes and neutrophils. Notably, there was no difference in the number of eosinophils between the Eth-treated and untreated

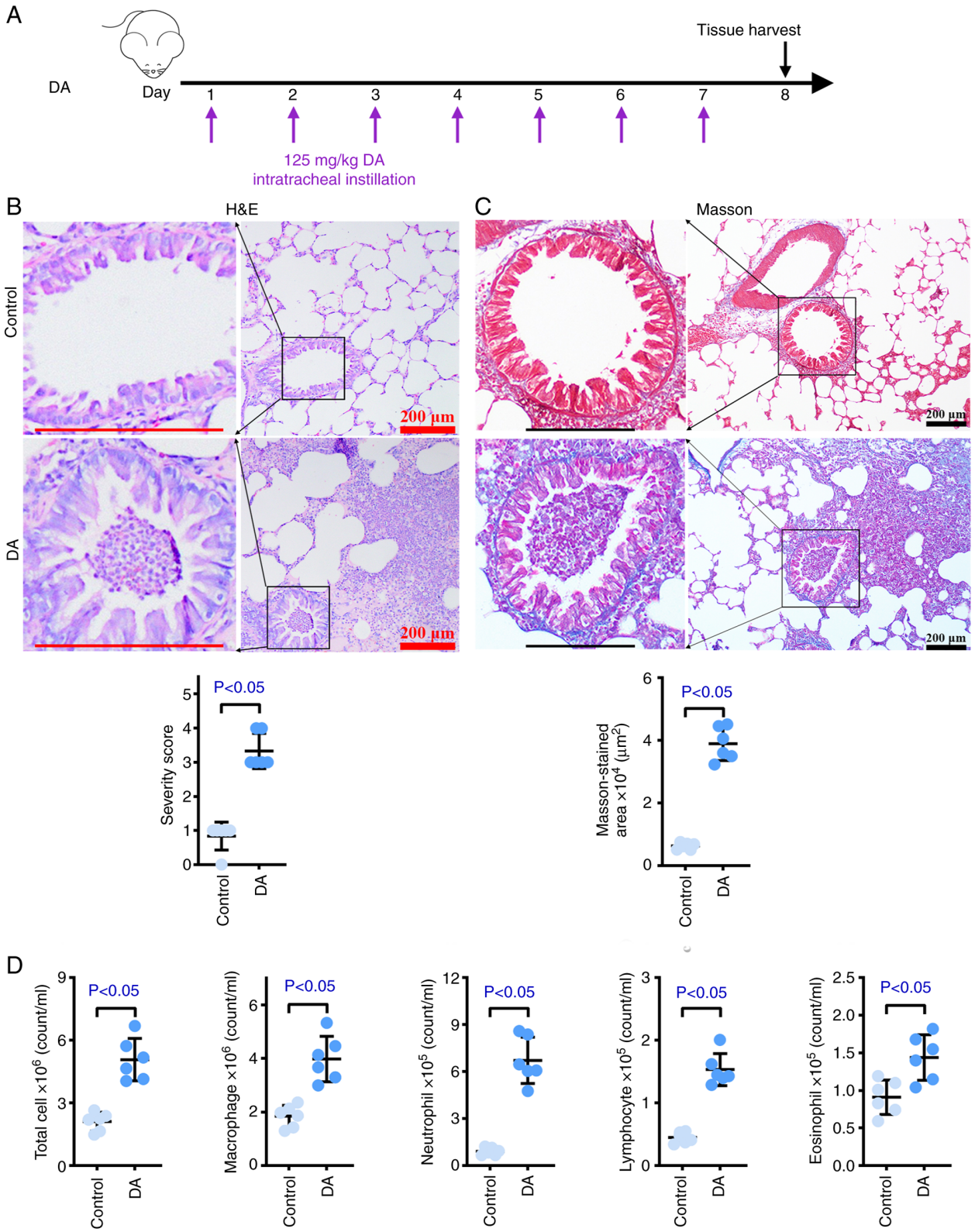

Figure 1. DA induces symptoms of BO in Sprague Dawley rats. Male Sprague Dawley rats accepted DA intratracheal instillation once a day for 7 days to generate the BO model. After DA intratracheal instillation on day 7, tissues were collected for the following experiments. (A) Animal experimental timeline. Representative (B) H&E and (C) Masson's trichrome-stained lung slices (scale bar: 200 μm). Quantitative analysis of severity is shown. (D) Bronchoalveolar lavage fluid total cell count, and macrophage, neutrophil, lymphocyte and eosinophil counts in control rats and DA-exposed rats. n=6. BO, bronchiolitis obliterans; DA, diacetyl; H&E, hematoxylin and eosin.

DA-induced rats. Western blotting and immunohistochemical analysis suggested that DA induced an increase in CIP2A, whereas Eth effectively reduced the protein expression levels of CIP2A (Fig. 4E and F). In addition, more occlusion was detected in the DA group, accompanied by an increase in CIP2A; by contrast, inhibition of CIP2A not only reduced the

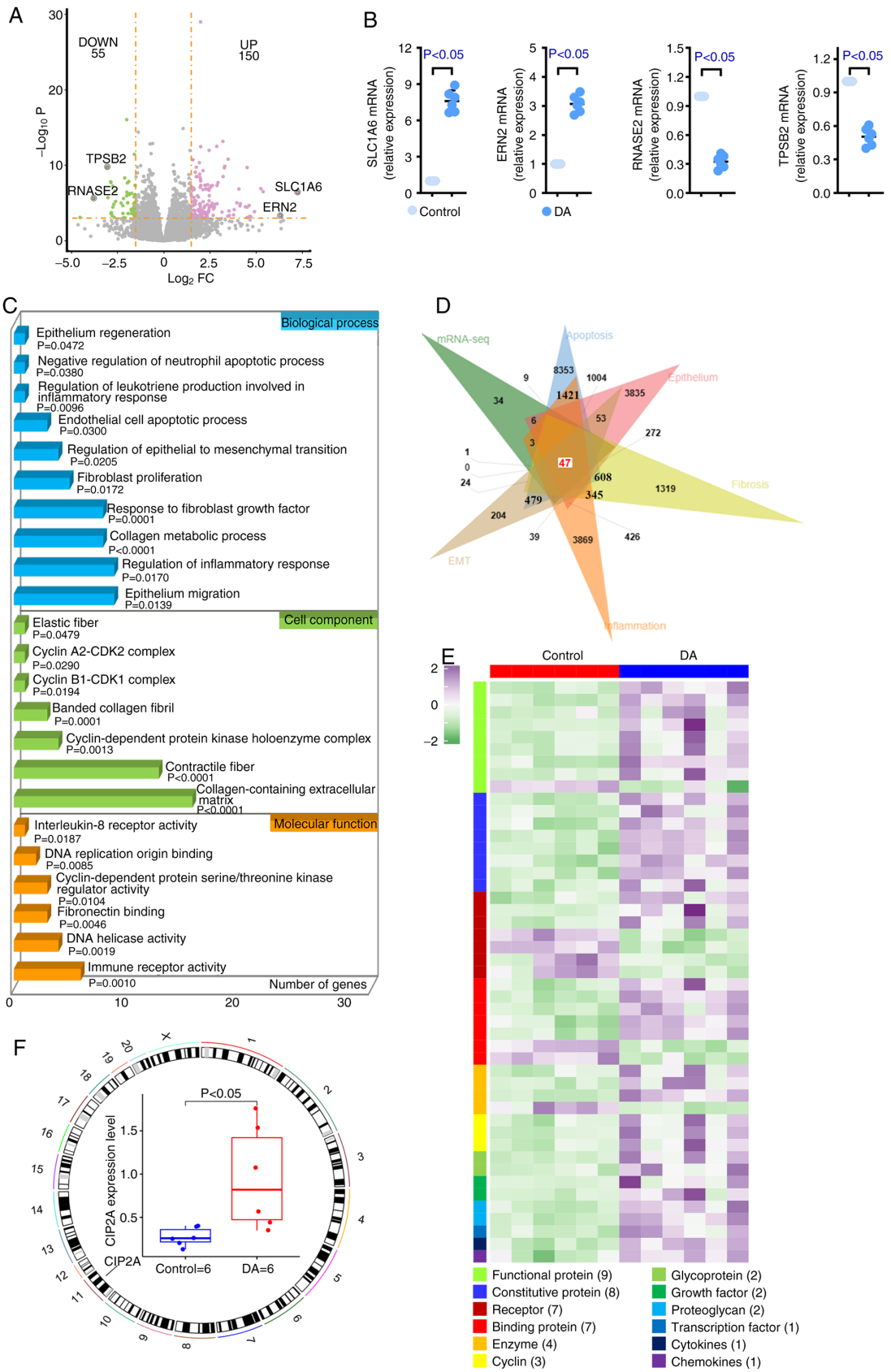

Figure 2. mRNA-seq of rat tissues. To explore the related molecular mechanism of bronchiolitis obliterans, high-throughput analysis was conducted using the lung tissues of rats. (A) DEGs in DA group rats relative to the control are shown using a volcano plot. DEGs were defined as an absolute value of log2FC >1.5 and adjusted-P<0.001. (B) Quantitative PCR was carried out to verify the results of mRNA-seq. Four DEGs were randomly selected for verification. (C) Gene Ontology analysis revealed that apoptosis, inflammation, fibrosis, EMT and epithelium-associated items were enriched by DEGs. (D) Venn diagram shows that 47 DEGs commonly existed in the six datasets. (E) Heatmap of 47 DEGs demonstrated that most genes were functional proteins. (F) CIP2A was located on chromosome 11 and was increased in DA-treated rats. n=6. CIP2A, cell proliferation regulating inhibitor of protein phosphatase 2A; DA, diacetyl; DEGs, differentially expressed genes; EMT, epithelial-mesenchymal transition; FC, fold change; mRNA-seq, mRNA-sequencing; SLC1A6, solute carrier family 1 member 6; ERN2, endoplasmic reticulum to nucleus signaling 2; RNASE2, ribonuclease A family member 2; TPSB2, tryptase β2.

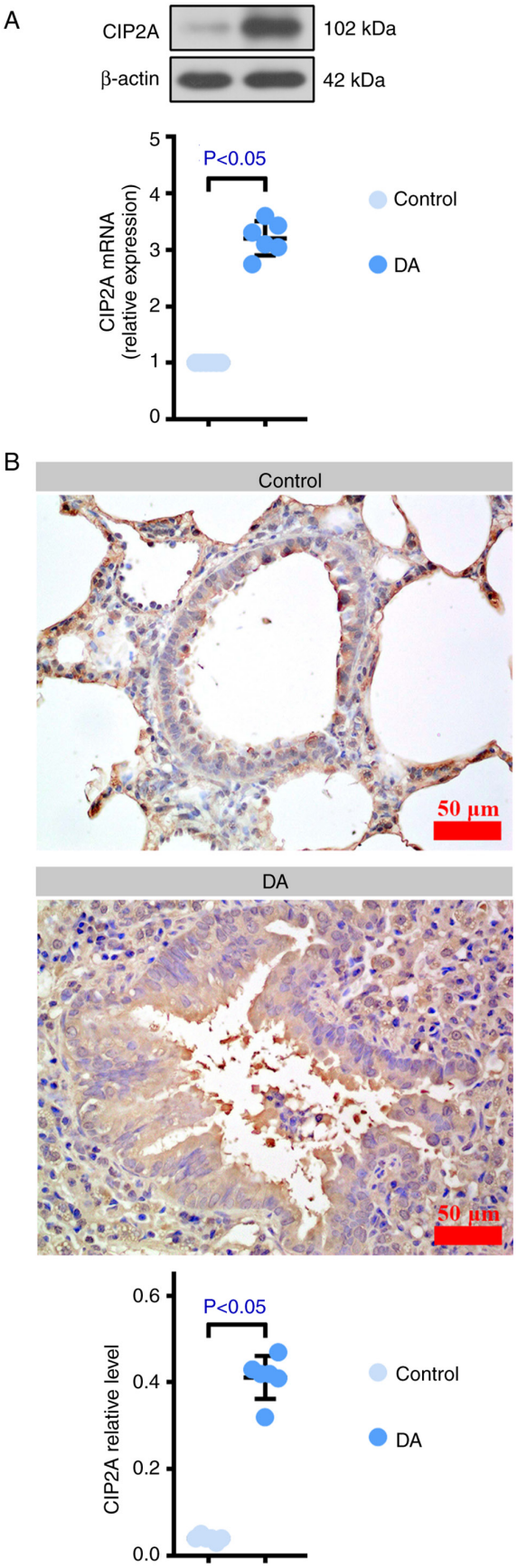

Figure 3. CIP2A expression is increased in DA group rats. (A) Quantitative PCR and western blotting, and (B) immunohistochemistry (scale bar: 50 μm) were used to detect the increased expression of CIP2A in samples from the DA group, which was initially determined by mRNA-sequencing. n=6. CIP2A, cell proliferation regulating inhibitor of protein phosphatase 2A; DA, diacetyl.

CIP2A levels but also decreased the occlusion area (Fig. 4F). Furthermore, stronger Vimentin and weaker E-cadherin expression were observed in BO model rats compared with in the control animals, whereas CIP2A inhibition reversed these results of immunofluorescence staining (Fig. 5A and B). In DA-treated rats, increased α-SMA, fibronectin, Snail and iNOS expression levels were detected compared with those in the control rats; by contrast, CIP2A inhibition reduced the expression levels of α-SMA, fibronectin, Snail and iNOS, as determined using western blotting (Fig. 5C). In addition, IL-1β, IL-6 and TNF-α levels were higher in BO model rats than those in the normal rats, whereas Eth suppressed these inflammatory factors (Fig. 5D). These data revealed that CIP2A reduction may contribute to relieve the fibrosis, EMT and inflammation caused by DA in rats.

Inhibiting CIP2A suppresses the NF-κB pathway in BO rats. The present study further investigated the pathway mediating the effects of CIP2A on BO development. After DA endotracheal instillation, increased p-IκBα and p65 nuclear translocation were observed; however, CIP2A inhibition attenuated the phosphorylation of IKBα and nuclear translocation of p65 (Fig. 6). Western blotting results suggested that CIP2A inhibition may suppress activation of the NF-κB pathway.

Inhibiting CIP2A reduces damage caused by DA in HPBECs. To explore the cellular mechanisms, the present study employed an *in vitro* cellular model of BO. The cells were treated with Eth after DA modeling. As depicted in Fig. 7A, CIP2A expression was reduced in response to Eth treatment in a dose-dependent manner. A concentration of 6 μM Eth exhibited the best inhibitory effect; therefore, this concentration was selected for subsequent experiments. The expression levels of α-SMA, fibronectin, Snail and iNOS were higher in DA-treated cells than in control HPBECs. By contrast, reduced α-SMA, fibronectin, Snail and iNOS levels were observed in DA + Eth-treated cells (Fig. 7B). As shown in Fig. 7D, the expression of Vimentin was promoted by DA, whereas E-cadherin exhibited the opposite trend. Inhibiting CIP2A weakened the expression of Vimentin and enhanced E-cadherin expression. Furthermore, DA increased the production of IL-1β, IL-6 and TNF-α, whereas CIP2A reduction deceased this elevation (Fig. 7C). These data demonstrated that CIP2A deficiency may inhibit the fibrosis, EMT and inflammation of DA-treated HPBECs.

Inhibiting CIP2A blocks the activation of NF-κB signaling in HPBECs. The present study further verified the effect of CIP2A on the NF-κB pathway *in vitro*. Western blotting suggested that DA induced an increase in CIP2A and Eth effectively reduced the protein expression levels of CIP2A in HPBECs (Fig. 8). The expression levels of p-IκBα and p65 nuclear translocation were increased by DA treatment compared with that in the control cells; however, CIP2A suppression decreased the phosphorylation of IκBα and nuclear translocation of p65 (Fig. 8). These results indicated that CIP2A may activate the NF-κB signaling pathway.

Discussion

In the present study, candidate genes that possibly participate in BO pathogenesis were detected by mRNA-seq in the

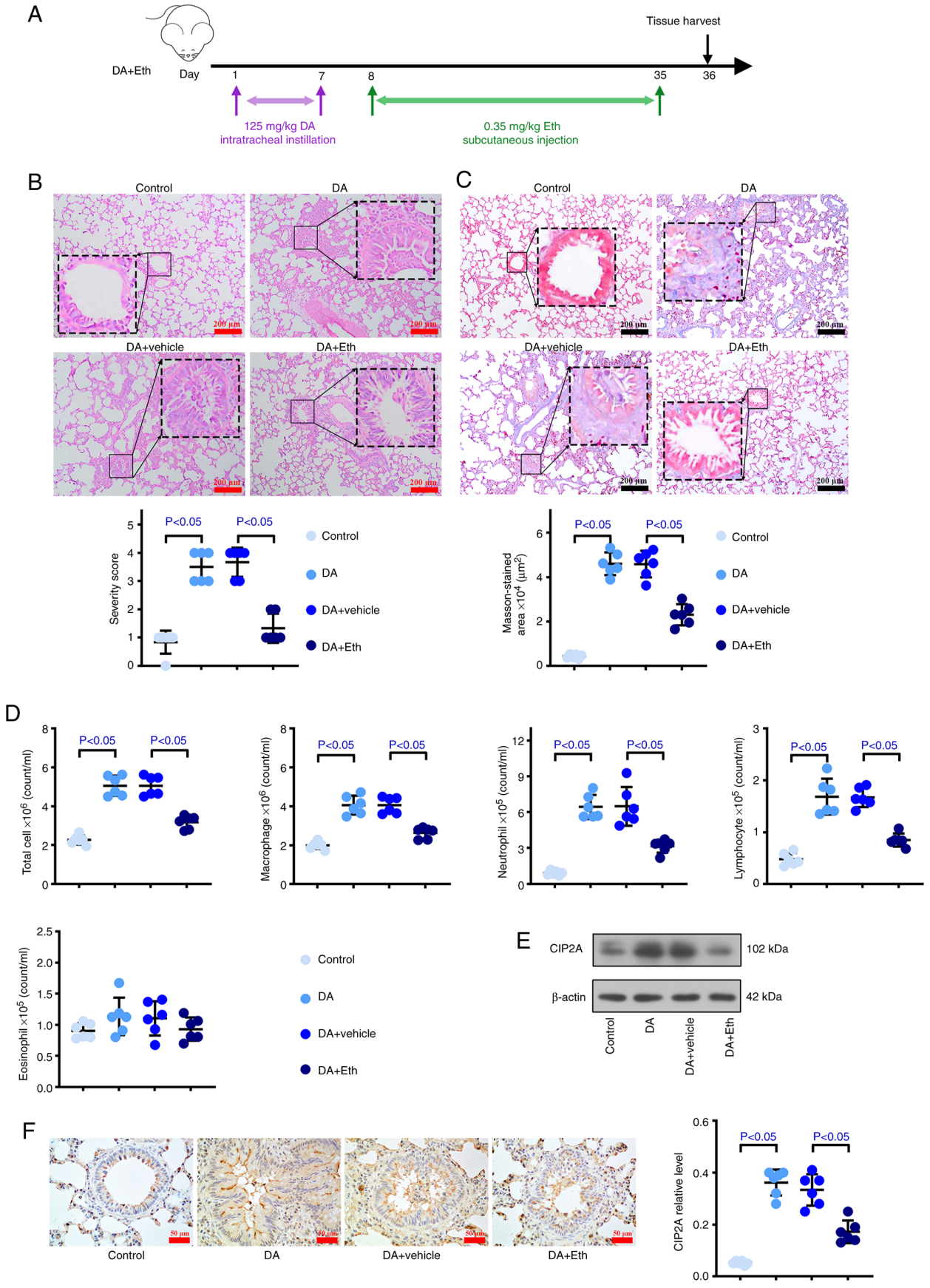

Figure 4. Inhibiting CIP2A attenuates the injuries induced by DA in the bronchi and lungs of rats. To evaluate the effect of CIP2A inhibition on bronchiolitis obliterans, Eth, a CIP2A inhibitor, was injected subcutaneously into DA group rats. (A) Animal experimental timeline. Representative (B) H&E and (C) Masson's trichrome-stained lung slices (scale bar: 200 μm). Quantitative analysis of severity is shown. (D) Bronchoalveolar lavage fluid total cell count, and macrophage, neutrophil, lymphocyte and eosinophil counts in the control rats, DA-exposed rats and Eth-treated DA-exposed rats. (E) Western blotting and (F) immunohistochemistry were used to measure the protein expression levels of CIP2A in lung tissues. n=6. CIP2A, cell proliferation regulating inhibitor of protein phosphatase 2A; DA, diacetyl; Eth, ethoxysanguinarine; H&E, hematoxylin and eosin.

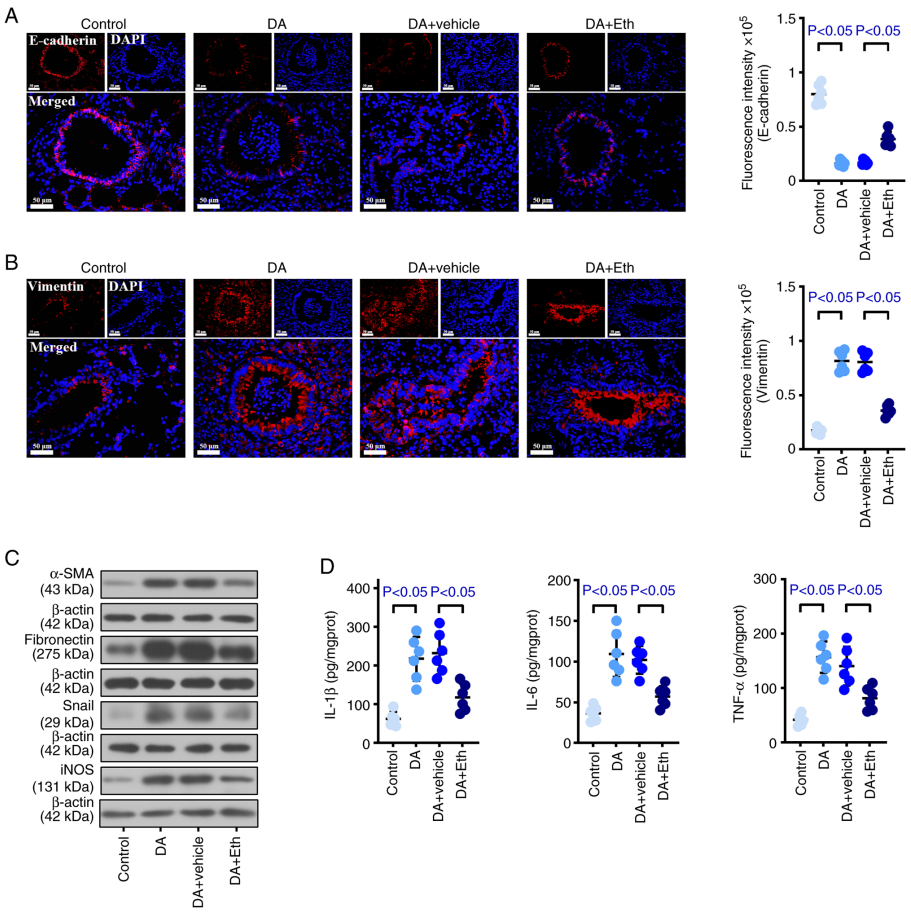

Figure 5. Inhibiting cell proliferation regulating inhibitor of protein phosphatase 2A weakens the epithelial-mesenchymal transition and inflammation induced by DA in the bronchi and lungs of rats. (A) E-cadherin and (B) Vimentin levels were detected by immunofluorescence (scale bar: 50 μm). (C) Western blotting was used to measure the protein expression levels of α-SMA, fibronectin, Snail and iNOS. (D) Enzyme-linked immunosorbent assay kits were used to analyze the levels of IL-1β, IL-6 and TNF-α. n=6. α-SMA, α-smooth muscle actin; CIP2A, cell proliferation regulating inhibitor of protein phosphatase 2A; DA, diacetyl; IL, interleukin; iNOS, inducible NO synthase; TNF-α, tumor necrosis factor-α.

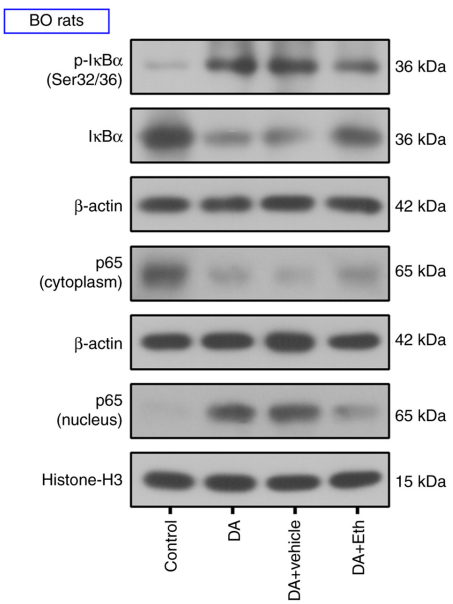

Figure 6. Inhibiting cell proliferation regulating inhibitor of protein phosphatase 2A suppresses the NF-κB pathway in rats with BO. The phosphorylation of IKBα and expression of p65 were assessed by western blotting. n=6. BO, bronchiolitis obliterans; DA, diacetyl; IκBα, inhibitor of NF-κB α; NF-κB, nuclear factor-κB; p-, phosphorylated.

tissues of rats with BO. Among them, CIP2A was increased and immunohistochemistry provided further information on the distribution of CIP2A in the affected lungs with bronchi. Notably, CIP2A aggravated the symptoms of BO *in vivo* and *in vitro*. These findings supported the association between CIP2A and BO development, and confirmed the preliminary results.

Due to multiple etiologies, a diverse clinical spectrum, various pathological appearances and the limited availability of animal models, effective treatments for BO are scarce and are usually disappointing (5,11). Once BO occurs, patients experience irreversible airflow obstruction, which ultimately develops into respiratory failure (11). Therefore, clarifying the mechanisms of BO progression and the identification of new targets is important. The present study established an animal model of BO using DA and demonstrated that this model replicated the pathological features of human patients with BO. Notably, more serious airway epithelial injury, larger inflammatory infiltration and fibrosis, more obvious blocking and more collagen deposition were observed in DA tissues with H&E and Masson's trichrome staining compared with those in the control tissues. However, the lack of physiological assessments of lung function is a limitation of the present study. Palmer *et al* (11) proposed that the obstruction

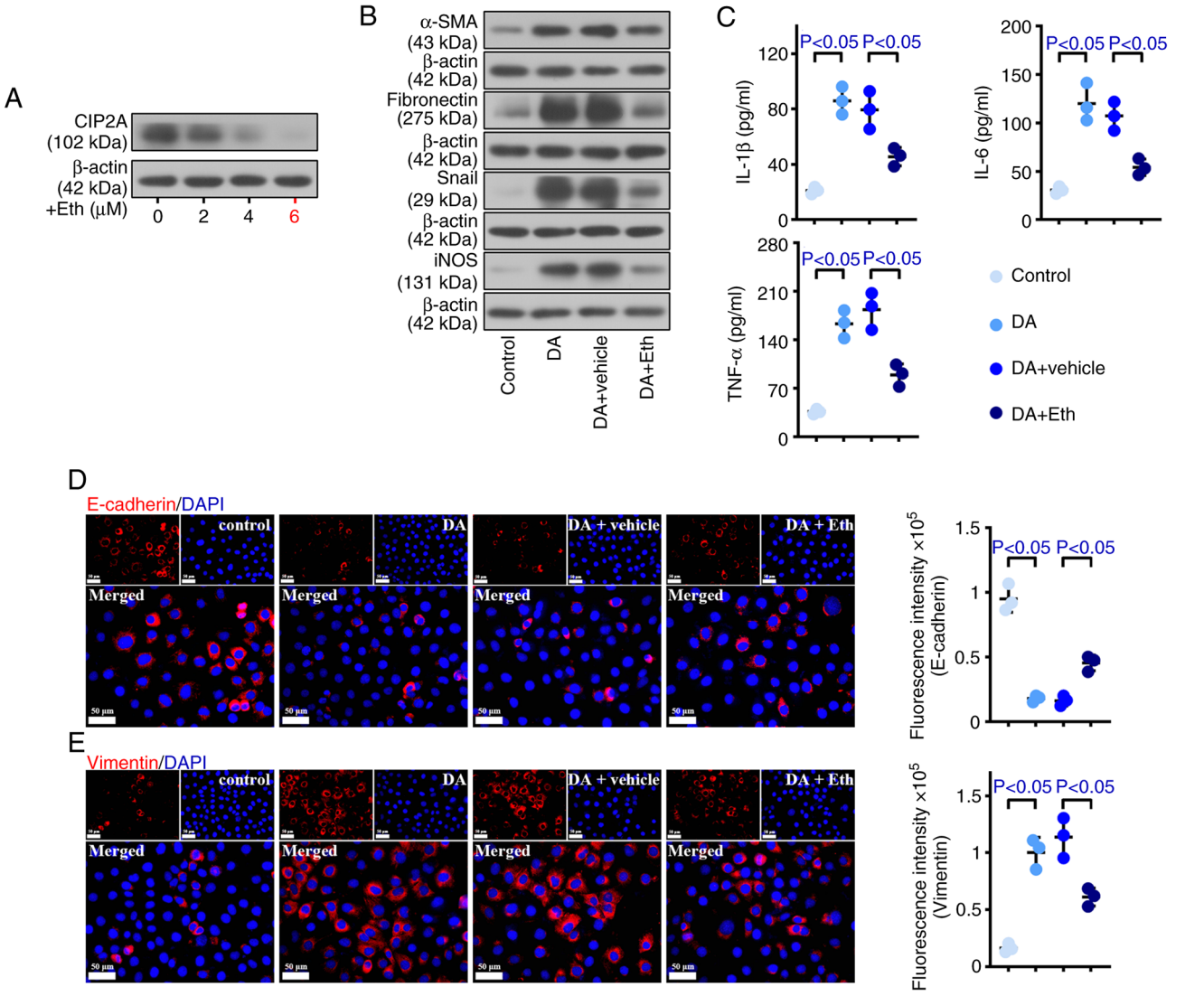

Figure 7. Inhibiting CIP2A reduces damage caused by DA in human primary bronchial epithelial cells. To explore the cellular mechanisms, an *in vitro* cellular model of bronchiolitis obliterans was employed. (A) Eth (6 μM) showed the best inhibitory effect on CIP2A expression. (B) Western blotting was used to measure the protein expression levels of α-SMA, fibronectin, Snail and iNOS. (C) Enzyme-linked immunosorbent assay kits were used to analyze the levels of IL-1β, IL-6 and TNF-α. (D) E-cadherin and (E) Vimentin levels were detected by immunofluorescence (scale bar: 50 μm). n=3. α-SMA, α-smooth muscle actin; CIP2A, cell proliferation regulating inhibitor of protein phosphatase 2A; DA, diacetyl; Eth, ethoxysanguinarine; IL, interleukin; iNOS, inducible NO synthase; TNF-α, tumor necrosis factor-α.

of airways may be caused by intraluminal granulation growth or intramural fibrosis. Considering the absence of knowledge regarding DA-induced BO, changes in the gene expression of rats treated with DA were assessed. The expression of the four genes (SLC1A6, ERN2, RNASE2 and TPSB2) that had the largest absolute value of log2FC, based on mRNA-seq data, were evaluated to verify the accuracy of the sequencing. The lack of further validation, such as validating the expression of the four genes in animal tissue samples by western blotting or immunohistochemistry, was a limitation of the current study.

GO analysis of DEGs revealed that DA-induced BO was associated with apoptosis, inflammation, fibrosis, EMT and the epithelium. Hence, GeneCards data were used to filter these relevant DEGs. CIP2A was not only significantly increased in DA samples but was also related to the aforementioned five aspects. Since its effect on BO was unknown, the present study assessed it. In the present study, the results of H&E and Masson's trichrome staining suggested that CIP2A inhibition ameliorated epithelial damage, inflammatory infiltration, fibrosis, blocking and collagen deposition in tissues from DA-treated rats. Fibrosis is defined as an excessive accumulation of collagen and fibronectin around damaged tissues (34). EMT is a process during which epithelial cells lose their original epithelial characteristics and gain mesenchymal features, which is characterized by decreased E-cadherin, and increased Vimentin and α-SMA (35-37). Facilitated EMT has been observed in patients with BO and animals accompanied by increased inflammation (7,38). In the present study, CIP2A suppression markedly affected the expression of EMT and fibrosis markers, as evidenced by increased E-cadherin, and reduced Vimentin, α-SMA, fibronectin and Snail expression. In cancer cells, inhibition of CIP2A has been shown to increase E-cadherin expression, but to suppress the expression of Snail and Vimentin, thereby restraining the

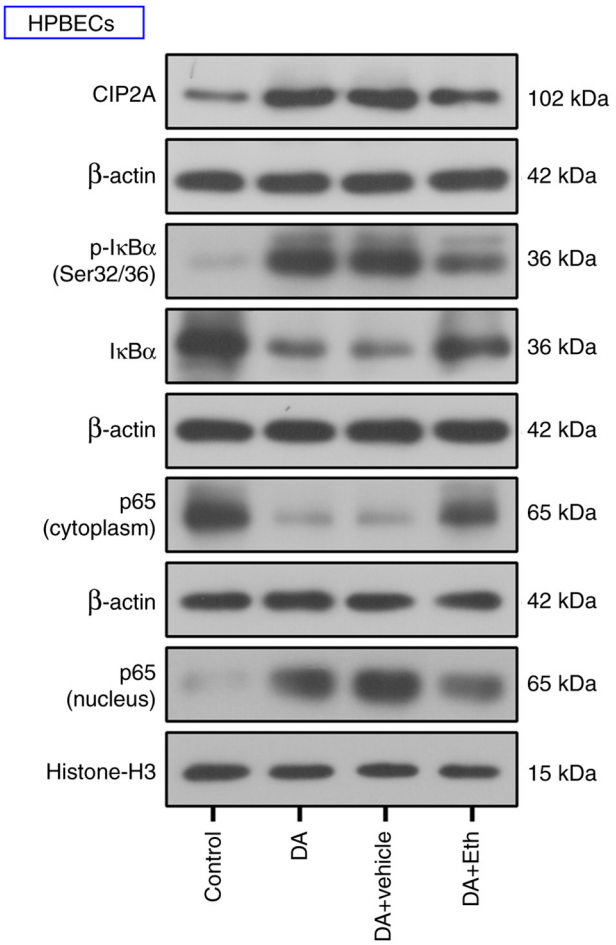

Figure 8. Inhibiting CIP2A blocks the activation of NF-κB signaling in HPBECs. The expression of CIP2A, and phosphorylation of IKBα and expression of p65 were assessed by western blotting. n=3. CIP2A, cell proliferation regulating inhibitor of protein phosphatase 2A; DA, diacetyl; HPBECs, human primary bronchial epithelial cells; IκBα, inhibitor of NF-κB α; NF-κB, nuclear factor-κB; p-, phosphorylated.

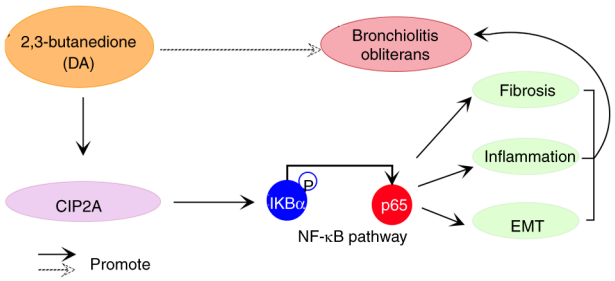

Figure 9. CIP2A promotes BO by activating the NF-κB pathway. BO is caused by DA and mediated by CIP2A. CIP2A deficiency inhibits fibrosis, inflammation and EMT in BO models through suppressing the NF-κB pathway. Solid and dashed arrows both indicate promotion. The solid arrow reveals the molecular mechanism through which the dashed arrow operates. BO, bronchiolitis obliterans; DA, diacetyl; CIP2A, cell proliferation regulating inhibitor of protein phosphatase 2A; EMT, epithelial-mesenchymal transition; NF-κB, nuclear factor-κB.

EMT process (21,39-41). Furthermore, CIP2A depletion has been reported to suppress fibronectin-accelerated cell proliferation (15). By contrast, overexpression of CIP2A may lead to enhanced levels of proinflammatory cytokines, including IL-1 and TNF-α, in aging-related chronic inflammation (42). In addition, downregulating CIP2A has been shown to result in devitalized cytokines, such as TNF-α, and decreased tissue damage and inflammatory cell infiltration, eventually inhibiting the progression of chronic obstructive pulmonary disease and lung cancer (43). In the present study, it was revealed that inhibition of CIP2A suppressed the levels of inflammatory factors, including IL-1β, IL-6, TNF-α and iNOS, in a model of BO after Eth treatment.

NF-κB is universally acknowledged to have an important role in inflammatory responses, which promotes downstream target gene expression and inflammatory mediator secretion when it is activated by stimuli (44,45). In addition, there are intricate connections between inflammation and fibrosis. TNF-α has been shown to accentuate transforming growth factor β1 (TGF-β1)-driven EMT, and TNF-α and TGF-β1 jointly activate TGF-β-activated kinase 1 and subsequently activate the NF-κB pathway. After a series of cascading reactions, EMT can be initiated, and inflammation and fibrosis are aggravated (46). In patients with BO, western blot analysis of NF-κB has been reported to be positive (47). Furthermore, activated NF-κB has been observed in samples from humans and animals with BO, and this activation may be associated with BO development (48-50). Notably, the current study observed that the NF-κB pathway was activated in DA-treated cells, accompanied by enhanced CIP2A levels, and that inhibition of CIP2A suppressed this activation, as evidenced by the restrained phosphorylation of IκBα and nuclear translocation of p65, suggesting that CIP2A may promote BO progression via the NF-κB pathway. In cancer, CIP2A has been reported to promote malignant biological behaviors of cancer cells through the AKT-mTOR (51,52), JNK (53) and GSK-3β/β-catenin (54) signaling pathways. CIP2A is also vital in osteoblast differentiation by causing ERK phosphorylation (55). However, whether CIP2A serves a role in BO through these pathways remains to be explored.

In conclusion, the present study demonstrated that BO may be caused by DA and mediated by CIP2A. Furthermore, CIP2A deficiency was shown to inhibit the fibrosis, inflammation and EMT of BO models through suppressing the NF-κB pathway (Fig. 9).

Acknowledgements

Not applicable.

Funding

This work was supported by the National Natural Science Foundation of China (grant no. 82104933).

Availability of data and materials

The mRNA-sequencing data generated in the present study may be found in the Gene Expression Omnibus under accession number GSE279398 or at the following URL: https://www.ncbi.nlm.nih.gov/geo/query/acc.cgi?acc=GSE279398. The other data generated in the present study may be requested from the corresponding author.

Authors' contributions

XuZ, XiZ, YL and BZ conceived the study. XuZ and YL designed the methodology. XuZ, XiZ and YL performed experiments and analyzed data. XuZ and BZ wrote and revised the manuscript. XuZ, XiZ and YL confirm the authenticity of all the raw data. All authors read and approved the final version of the manuscript.

Ethics approval and consent to participate

The present animal experiments were performed following the Guideline for the Care and Use of Laboratory Animals and were approved by the Experimental Animal Ethics Committee of Affiliated Hospital of Shandong University of Traditional Chinese Medicine [approval number: (2023) No. 163 application for provincial natural basic experiment]. Ethics approval for the use of the cells in the present study was waived.

Patient consent for publication

Not applicable.

Competing interests

The authors declare that they have no competing interests.

Authors' information

Corresponding author: Dr Xu Zhou ORCID: 0009-0002-8712-6732.

References

1. Chu CY, Kim SY, Pryhuber GS, Mariani TJ and McGraw MD: Single-cell resolution of human airway epithelial cells exposed to bronchiolitis obliterans-associated chemicals. Am J Physiol Lung Cell Mol Physiol 326: L135-Ll148, 2024.
2. Colom AJ and Teper AM: Post-infectious bronchiolitis obliterans. Pediatr Pulmonol 54: 212-219, 2018.
3. Flake GP and Morgan DL: Pathology of diacetyl and 2,3-pentanedione airway lesions in a rat model of obliterative bronchiolitis. Toxicology 388: 40-47, 2017.
4. Boehler A and Estenne M: Post-transplant bronchiolitis obliterans. Eur Respir J 22: 1007-1018, 2003.
5. Laohaburanakit P, Chan A and Allen RP: Bronchiolitis obliterans. Clin Rev Allergy Immunol 25: 259-274, 2003.
6. D'Amico R, Fusco R, Cordaro M, Siracusa R, Peritore AF, Gugliandolo E, Crupi R, Scuto M, Cuzzocrea S, Di Paola R and Impellizzeri D: Modulation of NLRP3 inflammasome through formyl peptide receptor 1 (Fpr-1) pathway as a new therapeutic target in bronchiolitis obliterans syndrome. Int J Mol Sci 21: 2144, 2020.
7. Zhang C, Niu Y, Yu L, Lv W, Xu H, Abuduwufuer A, Cao J and Hu J: The role of epithelial-mesenchymal transition in the post-lung transplantation bronchiolitis obliterans. J Cardiothorac Surg 12: 119, 2017.
8. Hakim A, Cooke KR, Pavletic SZ, Khalid M, Williams KM and Hashmi SK: Diagnosis and treatment of bronchiolitis obliterans syndrome accessible universally. Bone Marrow Transplant 54: 383-392, 2018.
9. Hodge S, Holmes M, Banerjee B, Musk M, Kicic A, Waterer G, Reynolds PN, Hodge G and Chambers DC: Posttransplant bronchiolitis obliterans syndrome is associated with bronchial epithelial to mesenchymal transition. Am J Transplant 9: 727-733, 2009.
10. Wang J, Kim SY, House E, Olson HM, Johnston CJ, Chalupa D, Hernady E, Mariani TJ, Clair G, Ansong C, *et al*: Repetitive diacetyl vapor exposure promotes ubiquitin proteasome stress and precedes bronchiolitis obliterans pathology. Arch Toxicol 95: 2469-2483, 2021.
11. Palmer SM, Flake GP, Kelly FL, Zhang HL, Nugent JL, Kirby PJ, Foley JF, Gwinn WM and Morgan DL: Severe airway epithelial injury, aberrant repair and bronchiolitis obliterans develops after diacetyl instillation in rats. PLoS One 6: e17644, 2011.
12. Kelly FL, Sun J, Fischer BM, Voynow JA, Kummarapurugu AB, Zhang HL, Nugent JL, Beasley RF, Martinu T and Gwinn WM: Diacetyl induces amphiregulin shedding in pulmonary epithelial cells and in experimental bronchiolitis obliterans. Am J Respir Cell Mol Biol 51: 568-574, 2014.
13. Kreiss K, Gomaa A, Kullman G, Fedan K, Simoes EJ and Enright PL: Clinical bronchiolitis obliterans in workers at a microwave-popcorn plant. N Engl J Med 347: 330-338, 2002.
14. van Rooy FGBGJ, Rooyackers JM, Prokop M, Houba R, Smit LAM and Heederik DJJ: Bronchiolitis obliterans syndrome in chemical workers producing diacetyl for food flavorings. Am J Respir Crit Care Med 176: 498-504, 2007.
15. Gao F, Xu T, Wang X, Zhong S, Chen S, Zhang M, Zhang X, Shen Y, Wang X, Xu C and Shen Z: CIP2A mediates fibronectin-induced bladder cancer cell proliferation by stabilizing β-catenin. J Exp Clin Cancer Res 36: 70, 2017.
16. Chen W, Liang JL, Zhou K, Zeng QL, Ye JW and Huang MJ: Effect of CIP2A and its mechanism of action in the malignant biological behavior of colorectal cancer. Cell Commun Signal 18: 67, 2020.
17. Laine A, Nagelli SG, Farrington C, Butt U, Cvrljevic AN, Vainonen JP, Feringa FM, Grönroos TJ, Gautam P, Khan S, *et al*: CIP2A interacts with TopBP1 and drives Basal-like breast cancer tumorigenesis. Cancer Res 81: 4319-4331, 2021.
18. Hu WT, Liuyang ZY, Tian Y, Liang JW, Zhang XL, Zhang HL, Wang G, Huo Y, Shentu YP, Wang JZ, *et al*: CIP2A deficiency promotes depression-like behaviors in mice through inhibition of dendritic arborization. EMBO Rep 23: e54911, 2022.
19. Zhou Y, Yang D, Chen H, Zheng C, Jiang H, Liu X, Huang X, Ye S, Song S, Jiang N, *et al*: Polyphyllin I attenuates cognitive impairments and reduces AD-like pathology through CIP2A-PP2A signaling pathway in 3XTg-AD mice. FASEB J 34: 16414-16431, 2020.
20. Zhou Y, Liu X, Ma S, Zhang N, Yang D, Wang L, Ye S, Zhang Q, Ruan J, Ma J, *et al*: ChK1 activation induces reactive astrogliosis through CIP2A/PP2A/STAT3 pathway in Alzheimer's disease. FASEB J 36: e22209, 2022.
21. Tang Q, Wang Q, Zeng G, Li Q, Jiang T, Zhang Z, Zheng W and Wang K: Overexpression of CIP2A in clear cell renal cell carcinoma promotes cellular epithelial-mesenchymal transition and is associated with poor prognosis. Oncol Rep 34: 2515-2522, 2015.
22. Wu Y, Gu TT and Zheng PS: CIP2A cooperates with H-Ras to promote epithelial-mesenchymal transition in cervical-cancer progression. Cancer Lett 356: 646-655, 2015.
23. Seppälä M, Tervo S, Pohjola K, Laranne J, Huhtala H, Toppila-Salmi S and Paavonen T: The association and prognostic relevance of cancerous inhibitor of protein phosphatase 2A and inflammation in tongue squamous cell carcinoma. APMIS 123: 1007-1015, 2015.
24. Nath S, Ohlmeyer M, Salathe MA, Poon J, Baumlin N, Foronjy RF and Geraghty P: Chronic Cigarette smoke exposure subdues PP2A activity by enhancing expression of the oncogene CIP2A. Am J Respir Cell Mol Biol 59: 695-705, 2018.
25. Jin L, Si Y, Hong X, Liu P, Zhu B, Yu H, Zhao X, Qin S, Xiong M, Liu Y, *et al*: Ethoxysanguinarine inhibits viability and induces apoptosis of colorectal cancer cells by inhibiting CIP2A. Int J Oncol 52: 1569-1578, 2018.
26. House EL, Kim SY, Johnston CJ, Groves AM, Hernady E, Misra RS and McGraw MD: Diacetyl vapor inhalation induces mixed, granulocytic lung inflammation with increased CD4+CD25+ T cells in the rat. Toxics 9: 359, 2021.
27. National Research Council Committee for the Update of the Guide for the C and Use of Laboratory A: The National Academies Collection: Reports funded by National Institutes of Health. In: Guide for the Care and Use of Laboratory Animals National Academies Press (US) Copyright © 2011, National Academy of Sciences., Washington (DC), 2011.
28. Love MI, Huber W and Anders S: Moderated estimation of fold change and dispersion for RNA-seq data with DESeq2. Genome Biol 15: 550, 2014.
29. Livak KJ and Schmittgen TD: Analysis of relative gene expression data using real-time quantitative PCR and the 2(-Delta Delta C(T)) method. Methods 25: 402-408, 2001.
30. Lin J, Deng H, Zhang Y, Zou L, Fu Z and Dai J: Effect of human umbilical cord-derived mesenchymal stem cells on murine model of bronchiolitis obliterans like injury. Pediatr Pulmonol 56: 129-137, 2021.

31. Ueno-Iio T, Shibakura M, Iio K, Tanimoto Y, Kanehiro A, Tanimoto M and Kataoka M: Effect of fudosteine, a cysteine derivative, on airway hyperresponsiveness, inflammation, and remodeling in a murine model of asthma. Life Sci 92: 1015-1023, 2013.
32. Foster MW, Gwinn WM, Kelly FL, Brass DM, Valente AM, Moseley MA, Thompson JW, Morgan DL and Palmer SM: Proteomic analysis of primary human airway epithelial cells exposed to the respiratory toxicant diacetyl. J Proteome Res 16: 538-549, 2017.
33. Liu Z, Ma L, Wen ZS, Cheng YX and Zhou GB: Ethoxysanguinarine induces inhibitory effects and downregulates CIP2A in lung cancer cells. ACS Med Chem Lett 5: 113-118, 2014.
34. Wynn TA and Ramalingam TR: Mechanisms of fibrosis: Therapeutic translation for fibrotic disease. Nat Med 18: 1028-1040, 2012.
35. Kalluri R: EMT: When epithelial cells decide to become mesenchymal-like cells. J Clin Invest 119: 1417-1419, 2009.
36. Kalluri R and Weinberg RA: The basics of epithelial-mesenchymal transition. J Clin Invest 119: 1420-1428, 2009.
37. Smith B and Bhowmick N: Role of EMT in metastasis and therapy resistance. J Clin Med 5: 17, 2016.
38. Borthwick LA, Parker SM, Brougham KA, Johnson GE, Gorowiec MR, Ward C, Lordan JL, Corris PA, Kirby JA and Fisher AJ: Epithelial to mesenchymal transition (EMT) and airway remodelling after human lung transplantation. Thorax 64: 770-777, 2009.
39. Chen XD, Tang SX, Zhang JH, Zhang LT and Wang YW: CIP2A, an oncoprotein, is associated with cell proliferation, invasion and migration in laryngeal carcinoma cells. Oncol Rep 38: 1005-1012, 2017.
40. Liu X, Sun Z, Deng J, Liu J, Ma K, Si Y, Zhang T, Feng T, Liu Y and Tan Y: Polyphyllin I inhibits invasion and epithelial-mesenchymal transition via CIP2A/PP2A/ERK signaling in prostate cancer. Int J Oncol 53: 1279-1288, 2018.
41. Zhang Y, Huang P, Liu X, Xiang Y, Zhang T, Wu Y, Xu J, Sun Z, Zhen W, Zhang L, *et al*: Polyphyllin I inhibits growth and invasion of cisplatin-resistant gastric cancer cells by partially inhibiting CIP2A/PP2A/Akt signaling axis. J Pharmacol Sci 137: 305-312, 2018.
42. Fujiki H, Sueoka E, Watanabe T, Komori A and Suganuma M: Cancer progression by the okadaic acid class of tumor promoters and endogenous protein inhibitors of PP2A, SET and CIP2A. J Cancer Res Clin Oncol 149: 9425-9433, 2023.
43. Nader CP, Cidem A, Verrills NM and Ammit AJ: Protein phosphatase 2A (PP2A): a key phosphatase in the progression of chronic obstructive pulmonary disease (COPD) to lung cancer. Respir Res 20: 222, 2019.
44. Marquardt JU, Gomez-Quiroz L, Arreguin Camacho LO, Pinna F, Lee YH, Kitade M, Domínguez MP, Castven D, Breuhahn K, Conner EA, *et al*: Curcumin effectively inhibits oncogenic NF-κB signaling and restrains stemness features in liver cancer. J Hepatol 63: 661-669, 2015.
45. Cai L, Ming D, Chen W, Zhao Y, Li Y, Sun W, Pi Y, Jiang X and Li X: Silybin alleviated hepatic injury by regulating redox balance, inflammatory response, and mitochondrial function in weaned piglets under Paraquat-induced oxidative stress. Antioxidants (Basel) 13: 324, 2024.
46. Gardner A, Fisher AJ, Richter C, Johnson GE, Moisey EJ, Brodlie M, Ward C, Krippner-Heidenreich A, Mann DA and Borthwick LA: The critical role of TAK1 in accentuated epithelial to mesenchymal transition in obliterative bronchiolitis after lung transplantation. Am J Pathol 180: 2293-2308, 2012.
47. Mohanakumar T, Sharma M, Bansal S, Ravichandran R, Smith MA and Bremner RM: A novel mechanism for immune regulation after human lung transplantation. J Thorac Cardiovasc Surg 157: 2096-2106, 2019.
48. Farivar AS, Mackinnon-Patterson B, Woolley S, Namkung J, Shimamoto A, Verrier ED and Mulligan MS: FR167653 reduces obliterative airway disease in rats. J Heart Lung Transplant 23: 985-992, 2004.
49. Farivar AS, Woolley SM, Naidu BV, Fraga CH, Byrne K, Thomas R, Salzman AL, Szabo CS and Mulligan MS: Poly (ADP) ribose synthetase inhibition reduces obliterative airway disease in rat tracheal allografts. J Heart Lung Transplant 23: 993-1002, 2004.
50. Ohmori K, Takeda S, Miyoshi S, Minami M, Nakane S, Ohta M, Sawa Y and Matsuda H: Attenuation of lung injury in allograft rejection using NF-κB decoy transfection-novel strategy for use in lung transplantation. Eur J Cardio-Thoracic Surg 27: 23-27, 2005.
51. Lei N, Peng B and Zhang JY: CIP2A regulates cell proliferation via the AKT signaling pathway in human lung cancer. Oncol Rep 32: 1689-1694, 2014.
52. Monga J, Suthar SK, Rohila D, Joseph A, Chauhan CS and Sharma M: (+)-Cyanidan-3-ol inhibits epidermoid squamous cell carcinoma growth via inhibiting AKT/mTOR signaling through modulating CIP2A-PP2A axis. Phytomedicine 101: 154116, 2022.
53. Peng B, Chai Y, Li Y, Liu X and Zhang J: CIP2A overexpression induces autoimmune response and enhances JNK signaling pathway in human lung cancer. BMC Cancer 15: 895, 2015.
54. Che Y, Zhang H, Li H and Wu X: CIP2A interacts with AKT1 to promote the malignant biological behaviors of oral squamous cell carcinoma by upregulating the GSK-3β/β-catenin pathway. Exp Ther Med 26: 514, 2023.
55. Son HE and Jang WG: Cip2A modulates osteogenic differentiation via the ERK-Runx2 pathway in MG63 cells. Biofactors 47: 658-664, 2021.